Colloidal stability of molten salt –based nanofluids: dynamic light scattering tests at high temperature conditions

Nuria Navarrete, Alexandra Gimeno-Furió, Josep Forner-Escrig, J. Enrique Juliá, Rosa Mondragón*

Departamento de Ingeniería Mecánica y Construcción, Universitat Jaume I, 12071-Castellón de la Plana, Spain

**Corresponding author: mondragn@uji.es*

ABSTRACT

The use of molten salt-based nanofluids as heat transfer fluids or thermal energy storage materials to increase the efficiency of Concentrated Solar Power plants has gained attention due to the use of the renewable energies against Global Warming. One of the issues of interest is the colloidal stability of the nanoparticles dispersed in ionic media like molten salts. In this work a new experimental set-up to measure the particle size distribution of molten salt-based nanofluids by means of Dynamic Light Scattering was developed. The colloidal stability of silica and Al/Cu nanoparticles dispersed in solar salt ($NaNO_3$-KNO_3) was experimentally measured for the first time. Silica nanoparticles were dispersed in water, calcium nitrate tetrahydrate and solar salt, and the formation of micrometrical agglomerates was observed when molten salts were used as base fluid due to the high ionic strength of the medium and the reduced Debye length. The influence of the nanoparticle composition was proved to be also important. For the Al/Cu metal alloy nanoparticles the agglomerates formed were smaller than for silica. Besides, even though both nanoparticles settle after 4h in static conditions, only Al/Cu nanoparticles recover the initial particle size distribution when they are mechanically redispersed.

Keywords: nanofluids; molten salts; colloidal stability; dynamic light scattering

1. Introduction

Solar energy has become the most important renewable energy source to reduce the consumption of fossil fuels and to mitigate Global Warming [1,2]. For high temperature applications, the solar radiation needs to be concentrated and the electricity generation can be achieved through Concentrated Solar Power (CSP) plants. One of the features that make CSP plants different from other renewable technologies is the ability to include a Thermal Energy Storage (TES) system in order to handle the intermittencies of solar availability and prevent the gap between energy supply and power demand [3].

Molten salts are widely used as Heat Transfer Fluid (HTF) as well as TES materials in Concentrated Solar Power plants (CSP) [4,5]. Solar Salt is the mixture of sodium and potassium nitrates (60-40wt%. respectively) commonly used in this industry. However, its thermal properties such as thermal conductivity and specific heat are worse than those of water. One of the actions gaining attention in the last years to increase the efficiency of the systems currently present in these industrial processes is the use of salt-based nanofluids to increase the thermal conductivity and specific heat of the molten salts [6-11]. Recently, the addition of nanoencapsulated phase change materials (nePCM) has been proposed to increase the overall thermal energy storage capacity thanks to the contribution of the latent heat of the nePCM [12-14].

A nanofluid is asuspension of solid particles with nanometrical size whose key property is its stability. Stability in colloid science is used not only in the thermodynamic sense but also in a strictly colloidal sense. Colloidally stable means that the colloidal particles do not settle or do not agglomerate at a significant rate [15]. Because of the small particle size of nanoparticles the displacement due to the Brownian motion overcomes the Stokes sedimentation providing stable suspensions.

For conventional nanofluids using non-ionic liquids as base fluid such as water, glycols or thermal oils, the DLVO (Dejarguin-Landau-Verwey-Overbeek) theory can be used to predict the stability of the nanofluids by knowing the total energy of interaction between two particles [16-18]. In the range of sizes of nanofluids, the particle-surface-to-particle-volume ratio is so high that all the interactions are controlled by short-range forces like Van der Waals attraction and surface forces. When nanoparticles come into contact, they will remain together unless a longer-range repulsive force acts to prevent particles from approaching each other. In aqueous media electrostatic repulsion is preferred. Electrostatic interactions between particles are due to the presence of surface charges appearing when particles are suspended in water. In non-aqueous media or dispersions of non-polar solids in aqueous media, steric repulsion is needed. In this mechanism, repulsion is achieved by means of the adsorption to the particle surface of polymeric chains or non-ionic surfactants that extend into the surrounding medium. However, the preferred and most effective stabilization mechanism involves electrosteric repulsion. In this case, both electrostatic and steric repulsion are combined, with the help of the addition of charged polymeric chains. Stabilization of nanofluids is performed by means of the addition of ionic surfactants (cationic or anionic) that generate a charged medium surrounding the polymeric chains adsorbed to the particle surface.

Studies of ionic liquids such as high-temperature inorganic molten salts and low-temperature organic salts (also known as IL) have shown that traditional stabilization mechanisms cannot explain the colloidal stability in this kind of highly concentrated electrolytes due to the strong electrostatic screening [19-21]. Therefore, for ionic liquids the stability depends on the chemical affinity between nanoparticle and base fluid. Indeed, it has been observed that stable salt-based nanofluids can be produced for

systems in which a new bonding is formed at the nanoparticle-fluid interface and the repulsive-oscillatory force of ionstructuring exceeds both the van der Waals and the double-layer electrostatic contributions by far.

One of the challenges when working with molten salt-based nanofluids is the direct measurement of the colloidal stability in molten state at high temperature [3]. Experimental techniques available include measurement of the evolution of nanoparticle size distribution with time by means of Dynamic Light Scattering (DLS) and the evolution of the light transmission through the sample at a fixed position. These techniques have been applied successfully for water and thermal oil based nanofluids [22-25]. However, the measurements were performed at low temperature (< 60ºC) due to the requirements of the available equipments.

Up to date colloidal stability of molten salt-based nanofluids has been mainly determined by means of visual observation of the nanofluid kept in a furnace for very long periods of time. Alternatively, it can be evaluated through the measurement over time of different physical properties influenced by the nanoparticles dispersion. Jo and Banerjee [26] checked the stability of a nanofluid sample by measuring its specific heat capacity for five consecutive melting–crystallization cycles, and no differences were found among them. Another method used to evaluate the settling of nanoparticles consists in keeping the molten salt–based nanofluid in a vial during a prolonged period of time at high temperature. After the solidification of the nanofluid, samples from the top and the bottom of the vial can be taken to measure and compare their specific heat capacity [9].

In this work, a new experimental set-up composed of an external, portable DLS system and a high temperature cuvette compatible with molten salts has been developed to measure the particle size distribution of the nanoparticles suspended at high temperature

conditions up to 500ºC. In order to calibrate the device, silica nanoparticles were first dispersed in water and calcium nitrate tetrahydrate (melting point 42.7ºC) and the results were compared to measurements carried out in a commercially available equipment working up to 90ºC. Then, solar salt-based nanofluids were prepared and the colloidal stability of silica and Al/Cu nanoencapsulated phase change material was measured. The influence of the base fluid and the chemical composition of the nanoparticle were evaluated showing the instability of the nanoparticles in ionic fluids. Al/Cu nanoencapsulated phase change material showed the best behaviour as the initial particle size distribution is recovered when the nanofluid is mechanically redispersed after 4h in static conditions.

2. Materials and sample preparation

Different combinations of nanoparticles and base fluids were used for the production of nanofluids. Three nanofluids with silica nanoparticles were created using distilled water, $Ca(NO_3)_2$ and Solar salt as the base fluids. A different nanofluid containing Solar salt and nanoparticles consisting of a metallic Al/Cu alloy was also prepared.

The nanoparticle concentration used for all the nanofluids was 0.46% in volume. Despite being a rather high loading for DLS measurements, this was tested to be a suitable concentration for measuring particle size and clustering behaviour being the solid load similar to real nanofluid applications.

The silica used for the nanofluids was obtained from a commercial suspension (Ludox SM-30, 30 wt% suspension in water, Sigma Aldrich). These are particles well dispersed in water with a narrow size distribution. Three different nanofluids were prepared with silica nanoparticles. For the one using water as the base fluid, the corresponding volume of silica solution was added to 100ml of distilled water to obtain the desired

concentration of 0.46 v%. The nanofluid was then dispersed using an ultrasonic probe (Sonopuls HD2200, Bandelin, HF-output of 200 W and HF-frequency of 20 kHz) during 3 min at 100%. It was previously tested that these conditions are optimal for homogenization of samples of this volume with high energy input systems [18]. The improvements after this time are negligible and it avoids excessive heating of the fluid due to the sonication.

For the synthesis of the $Ca(NO_3)_2$ based nanofluid, the nitrate (Calcium nitrate tetrahydrate, ACS reagent, 99-103%, Sigma Aldrich) was previously left overnight in an oven at 80ºC in order to avoid any possible moisture, since its deliquescence is very high. The melting point of the nitrate is 42.7ºC and it can be handled in liquid phase at relatively low temperatures. The silica in solution was added to the molten nitrate and mixed with a magnetical stirrer and then put back in the oven to remove the water contained in the Ludox suspension. After that, it was let cool down to 60ºC in order to be able to use the ultrasonic probe while it remained in melted state. The nanofluid was sonicated during 3 min at 100%.

Solar salt is the name given to the mixture of $NaNO_3$ and KNO_3 commonly used in the solar thermal industry. $NaNO_3$ (Analytical grade ACS, Labkem) and KNO_3 (Extra pure, Scharlau) were mixed in a 60:40wt proportion and the nanoparticles were added and hand-mixed. In the case of the silica nanofluid, the mixture was introduced in an oven at 100ºC to remove the water from the Ludox suspension. The nanoparticles were dispersed in both nanofluids (containing silica and Al/Cu nanoparticles) by melting the mixture at 300ºC and using a mechanical stirrer that consists of a rotating engine connected to a blade. The mixtures were stirred for 10 minutes at 1000rpm and then immediately cooled in the form of pellets.

Al/Cu nanoparticles were commercially obtained from Advanced Powder Technologies LLC. They consist of particles of an Aluminium-Copper alloy in an 80%Al-20%Cu weight percentage. They are produced by the wire explosion in inert gas method, what makes their size distribution wide, presenting particles that can reach from 20 up to 300 nm in diameter.

For the zeta potential measurements, nanoparticles were dispersed in an aqueous solution containing 1% of dissolved solar salt. Dispersion was made by applying 1 min of sonication with the ultrasound probe aforementioned. The pH value was modified adding NaOH and HCl solutions at 10 wt%.

3. Experimental techniques

3.1 TEM

The silica and Al/Cu primary nanoparticles were observed using Transmission Electron Microscopy (TEM) imaging. Images were taken with an electronic microscope (TEM, JEOL-JEM 2100) operating at an accelerating voltage of 200 kV. The morphology and the primary particle size were studied. These images were then processed to measure the diameters of over 1000 particles and to obtain the particle size distribution.

3.2 DLS

The stability of the nanofluids has been analysed using two different Dynamic Light Scattering systems. This technique measures the light scattered by the particles due to their Brownian motion, and associates its intensity with their size.

The silica nanofluids with water and $Ca(NO_3)_2$ as base fluids have been measured with a Malvern ZetaSizer Nano. This device is commonly used to measure particle size distributions in colloidal suspensions and nanofluids by means of Dynamic Light Scattering (DLS). The equipment is composed of a laser, that illuminates the cell

containing the sample, and a detector that acquires the intensity of the light scattered by the particles suspended. Both the laser and detector are enclosed in the device, and the hydrodynamic diameter is calculated based on the intensity of the scattered light at 173º. ZetaSizer has an incorporated heating system that allows the samples to be heated up to 90ºC. Samples of 1ml are tested in a quartz cell and data is acquired in three sets of 90 seconds each. The distributions of those three datasets are then compared to check their similarity and averaged.

In order to measure the particle size distribution of molten salt-based nanofluids at high temperature conditions a new system was developed. A DLS device VASCO FLEX particle size analyser (Cordouan Technologies) consisting of an external laser head that contains the light emitter and receiver was used (65mW-658nm fiber pigtailed laser). The light registered corresponds to backscattering with an angle of 170º. In order to heat up and control the temperature of the samples, a high temperature cuvette was designed. It consists of a cylindrical stainless steel cuvette with two fused quartz windows on the sides with a 20 ml sample volume. A heating ring is installed around the cuvette and two K-thermocouples are used to control the temperature on the wall of the cuvette and inside the fluid. The maximum working temperature of this system is 500ºC. A camera and lighting system is also available to take images of the fluid evolution inside the cuvette. A more detailed scheme of this experimental set-up can be observed in Figure 1.

For the calibration of the new DLS system, water and calcium nitrate silica nanofluids were simultaneously measured with the ZetaSizer and the VASCO FLEX DLS systems respectively at 25ºC and 80ºC. Stability of the solar salt-based nanofluids was also studied with VASCO FLEX DLS system. Particle/cluster size was measured

periodically during a 4-hour period for each of the samples, in order to observe the aggregation and sedimentation of the particles.

A refractive index of 1.46 and a viscosity of 23.093cP were used for $Ca(NO_3)_2$ at 80ºC. For Solar salt a refractive index of 1.41 and a viscosity of 8.5cP were used based on previous measurements.

3.3 Zeta potential

The zeta potential was measured at 25ºC using a Zetasizer Nano ZS (Malvern Instruments Ltd., UK) from the electrophoretic mobility of particles when an electric field is applied. This velocity is measured using Laser Doppler Velocimetry (LDV) and the zeta potential is obtained through the Henry equation.

4. Results and discussion

4.1 External Dynamic Light Scattering system set-up and configuration.

Initially, the VASCO FLEX external DLS system has been calibrated at low temperature in order to ensure the reliability of the results obtained in high temperature conditions. For that purpose, a comparison of the results obtained from the external system coupled to the heated cuvette and the closed DLS system, Malvern ZetaSizer, widely used in literature, has been carried out. Different nanofluids based on silica nanoparticles have been analysed. These particles were commercially obtained and present a narrow size distribution centred on 25 nm. Two different nanofluids were initially synthesized using water and $Ca(NO_3)_2$ as base fluids, with nanoparticle volume loadings of 0.46%.

The results obtained from these analyses are depicted in Figure 2 and presented in Table 1. All the samples were measured in both DLS systems. The nanofluid based on water was studied at room temperature and at 80ºC, whereas the one based on $Ca(NO_3)_2$ was

only analysed at 80ºC, since the melting temperature of calcium nitrate tetrahydrate is 42.7ºC.

In Figure 2, it is observed that the particle distributions obtained in water nanofluids are almost identical for both DLS systems and that the differences for both temperatures are negligible. Both results obtained for the $Ca(NO_3)_2$ are also very similar. However, it should be taken into account that the longer stabilization times in the ZetaSizer and the better resolution of the VASCO FLEX cause a smaller peak to be measured with the latter but not with the former.

In Table 1, $D_{i,50}$ of all the samples is compared. $D_{i,50}$ refers to the hydrodynamic diameter for which 50% of the scattered light comes from particles or particle clusters smaller than it. Small deviations exist among the measurements of all of the nanofluids studied. Thus, the reliability of the external DLS measuring system has been proven for both aqueous and ionic medium, as well as for different temperatures.

However, a great deviation is present between different base fluids, and particles are noticeably more aggregated within the nitrate salt. This phenomenon is due to the ionic charge of the medium and its influence on the colloidal stability of the nanoparticles suspended in it as it will be discussed later.

4.2 Colloidal stability

There are several forces that determine the stability of nanofluids. Among them, Stokes sedimentation due to gravity and diffusivity due to Brownian motion can be used to calculate the colloidal stability limit of a suspension [27]. The colloidal stability limit is the critical size of a particle or particles' cluster for which the displacement due to the Brownian motion equals the one due to the Stokes sedimentation. Thus, if they have bigger dimensions than the colloidal limit the Stokes sedimentation becomes

predominant and the particles will settle being the nanofluid not stable through time. The diffusion of a particle due to Brownian motion can be calculated through Equation 1:

$$X = \left[t \frac{kT}{3\pi\eta a} \right]^{\frac{1}{2}} \qquad \text{Equation 1}$$

where t is time in seconds, k is Boltzmann's constant, T is temperature in Kelvin, η is the viscosity of the suspending fluid, and a is the particle radius.

On the other hand, the displacement due to the Stokes sedimentation can be calculated as shown in Equation 2:

$$X = \frac{2a^2(\rho_p - \rho_f)gt}{9\eta} \qquad \text{Equation 2}$$

where ρ_p is the density of the particle, ρ_f is the density of the base fluid and g is the acceleration due to gravity.

The intersection between both parameters determine the colloidal limit for a particular combination of particle and base fluid, as it can be observed in Figure 3, where they have been calculated for different nanofluids including combinations of water, $Ca(NO_3)_2$ and Solar salt as base fluids and silica and Al/Cu nanoparticles for the latter. The temperatures chosen vary according to the base fluid, being 25ºC and 80ºC for the water based nanofluids, 80ºC for the $Ca(NO_3)_2$ based one, and 250ºC and 300ºC for the Solar Salt. All the calculations have been made for a time of 300s.

In Figure 3 a), it is noticed that the colloidal limit in water is smaller for higher temperatures. Attending also to Figure 3 b), c) and d), it is concluded that the colloidal

limit is higher for the silica nanoparticles immersed in ionic liquids (circa 400nm for both $Ca(NO_3)_2$ and Solar salt) than in water, and also that it is smaller for the Al/Cu nanoparticles than the silica ones in Solar salt. Therefore, further stability will depend significantly on the cluster size achieved in the production process of the nanofluid.

Silica and Al/Cu metal alloy nanoparticles were used to analyse the influence of the base fluid and the nanoparticle composition on the colloidal stability. TEM micrographs of the nanoparticles are shown in Figure 4 in which the primary particle size can be observed.

Initially, experimental DLS measurements have been made for the silica nanoparticles immersed in different base fluids in order to determine the influence of the latter in particle agglomeration. The particle size distribution of the primary silica nanoparticles alone has also been studied by TEM imaging. In Figure 5, the results of this study are presented. It can be noticed that the initial size of the particles analysed by TEM imaging ranges from 12 to 36 nm, whereas the diameters detected in all the nanofluids are bigger. This feature shows that there is a certain amount of agglomeration for all the base fluids, but also that it is considerably higher for molten salts than for water. Regarding the nanofluid based on Solar salt, it is also observed that some particle clusters are presumably out of the measuring range, as they are bigger than 10000 nm.

The agglomeration state achieved when the same nanoparticles are dispersed in different base fluids can be explained from the interaction forces acting on the solid-fluid system. For all the nanofluids tested that contain silica nanoparticles, the Van der Waals attraction forces depending on the Hamaker constant (A_{eff}= $6.3 \cdot 10^{-21}$J) will be similar, while the electrostatic repulsion forces, depending on the surface charge and the thickness of the electrical double layer (Debye length), will be the ones causing the final agglomeration state.

In Table 2, some parameters related to the electrical double layer thickness are compared to the sizes obtained in the DLS analysis. According to Debye-Hückel theory, an electrical double layer is formed whenever a solid-liquid interface exists as shown in Figure 6 [28]. These are structures that appear in the solid surface, since the ions are ordered around it in the first layer due to surface charge phenomena and in the second layer because of the attraction of these first layer ions, electrically screening them. The existence of this double layer of ions surrounding every particle can be of use for stability purposes, as there are repulsion forces between the ions in the external layers of different particles. Overlap of the electrical double layers associated with two surfaces leads to an increase in the ionic concentration. The osmotic pressure that results from the increased concentration acts to push the surfaces apart.

In Table 2, the electrical double layer thickness has been then calculated according to the Equation 3 [29]:

$$\boldsymbol{\kappa^{-1}} = \left[\frac{\boldsymbol{\varepsilon\varepsilon_0 RT}}{\boldsymbol{F^2 2I}}\right]^{\frac{1}{2}} \qquad \text{Equation 3}$$

where κ^{-1} is the double layer thickness, ε is the dielectrical constant of the medium, R is the ideal gas constant, T is the absolute temperature, F is Faraday's constant and I is the ionic strength of the medium.

The ionic strength of the medium, for molten salt based nanofluids was calculated by means of the following equation:

$$\boldsymbol{I} = \frac{\boldsymbol{1}}{\boldsymbol{2}}\sum \boldsymbol{c_i \cdot z_i^2} \qquad \text{Equation 4}$$

where c_i is the concentration of the ions present and z_i is their ionic charge.

For water based nanofluids containing small amounts of electrolytes already present in the water, the empirical equation from Griffin and Jurinak [30], which permits to obtain the ionic strength from electrical conductivity measurements is:

$$\boldsymbol{I = 0.013 \cdot EC} \qquad \text{Equation 5}$$

It is observed that as the ionic strength of the medium increases, the thickness of the electrical double layer decreases, and so the particles are more likely to agglomerate. This is in accordance with the size data obtained from DLS analyses, where a drastic increase in the clusters sizes can be noticed for the molten salt-based fluids, in which the ionic strength is greatly superior to that of water. It can also be observed that for divalent salts (Ca^{+2}) the ionic strength is higher and therefore the Debye length is lower leading to the formation of micrometrical agglomerates mainly. For the solar salt (monovalent salts) nanoparticles agglomerate having similar intensities and thus population of nanometrical and micrometrical clusters.

Furthermore, the evolution of agglomeration has been tested for the two nanofluids based on Solar salt in order to compare the effect of the different nanoparticles on the stability. The fluids have been periodically analysed during 4 hours. The nanofluids have been mechanically redispersed after the test to check if it was possible to recover the initial particle size distribution. These analyses are depicted in Figures 7, 8 and 10.

In Figure 7 a) and b), the initial, final and after redispersion particle size distributions for both nanofluids at 250ºC are shown. It can be noticed that the cluster sizes are generally bigger in the silica nanofluid than for the Al/Cu. In both cases, clusters of nanoparticles whose size is bigger than the stability limit previously obtained are initially present indicating that nanoparticles will settle and the nanofluid will not be stable. In addition, it can be deduced from the figure that part of the clusters in the silica

nanofluid after 4h are above 10000 nm, so they do not appear in the analysis until they are redispersed, their size becomes smaller and they can be detected again by the DLS system.

Figure 7 c) and d) show the evolution of the main peaks of the size distribution through time and after redispersion. As the size distributions were not monomonal and a mean particle size cannot be used, it was plotted the size of the peaks obtained at any measured time. Bigger bubbles correspond to higher intensity peaks detected, namely, a higher number of clusters of that size. It is observed that for the silica nanofluid the clusters are generally bigger. It also should be taken into account that when peaks appear around the limit of 10000 nm, part of the clusters are out of the measurement range, so the DLS equipment is only able to detect the smaller ones, leading to artefacts in which the apparent size of the sample is smaller. This artefacts can be observed around 100 min, where it seems like the highest peak of the size distribution has decreased, but it is only due to the biggest clusters falling out of the measurement range. On the other hand, the nanofluid with Al/Cu nanoparticles presents smaller sizes in general, although there is an increase starting at 45 minutes. Although both nanoparticles lead to unstable nanofluids, the one containing Al/Cu presents smaller cluster sizes and the agglomeration rate is lower. Besides, after the redispersion, both nanofluids effectively reduce the cluster sizes very close to the initial state, proving that mechanical stirring and the high shear conditions applied are suitable to break bigger agglomerates into smaller ones instead of promoting agglomeration.

In order to study the influence of the temperature on the stability, the same analysis has been done for the Solar salt based nanofluids at 300ºC. The results are depicted in Figure 8. In Figure 8 a) and b), similar results to the obtained at 250ºC are registered. The silica cluster sizes are initially bigger than the Al/Cu ones, and this difference is

higher than for the lower temperature. Also, the amount of clusters with sizes above 10000 nm after 4h is assumed to be bigger than for 250ºC, based on the higher intensity of the peak for this size. As expected, at higher temperature the fluid viscosity decreases while the Brownian motion is increases promoting the contact and agglomeration of the nanoparticles. In Figure 8 c) and d), smaller clusters are registered for the nanofluid with Al/Cu nanoparticles, although there is an increase starting at 45 minutes, when most of the clusters appear to have sizes around 1500 nm. This increase was also registered for the nanofluid at 250ºC. The Al/Cu nanofluid presents also at 300ºC a lower agglomeration rate than the silica one. Finally, after the redispersion, the Al/Cu nanofluid effectively reduces the cluster sizes very close to the initial state, which does not occur in the silica nanofluid.

It is obvious that the chemical composition of the nanoparticle influences the solid-liquid interactions leading to different behaviours in stability. The two main parameters influencing the interaction forces that depend on the nanofluid composition are the Hamaker constant (related to atractive force) and the particle surface charge or zeta potential (related to electrostatic repulsive force) [31, 32]. Regarding the Hamaker constant, its value for silica nanoparticles can be found in the literature but in the case of the Al/Cu nanoparticles it is difficult to determine. Although the core of the nanoparticles is composed by a known alloy, nanoparticles are encapsulated by an oxide shell as observed in Figure 4. This shell is assumed to be composed mainly of aliminium oxide and formed naturally by passivation of the metal but no exact composition and properties can be obtained to determine the nanoparticle behaviour. Therefore, real values for the Hamaker constant and the Van der Waals atractive force cannot be obtained but they are expected to be different due to the different chemical composition of the nanoparticles.

Regarding the particle surface charge, the zeta potencial and the point zero charge (or isoelectic point) of the nanoparticles also depends on the particle composition. From the best of the authors knowledge it is not possible to measure the zeta potential of nanoparticles dispersed in molten solar salt due to the high melting point. In spite of this the effect of the composition on the zeta potential behaviour was measured dispersing both nanoparticles in an aqueous solution containing a 1% of solar salt disolved. It is known that the presence of electrolytes produces a screening effect reducing the surface charge so both nanoparticles were tested under the presence of small concentrations of salt. In Figure 9 the evolution of the zeta potential for both samples with pH is shown. For silica nanoparticles the isoelectric point was achieved at pH values close to 2, similar to that found in the literature. For the Al/Cu nanoparticles the isoelectric point was found at pH values close to 7 indicating that the surface composition is formed mainly of aliminium oxide whose values reported in the literature are close to 8. The differences found in the isoelectric point leads to a different behaviour and stability when dispersed in the same fluid media. It can be also observed that for the higher charged conditions (extreme pH values) the Al/Cu nanoparticles present a sharp slope with higher zeta potential than the silica ones and thus the stability is expected to be higher in agreement with the DLS measurements. In addition, it has to be mentioned that the production process of both nanofluids is different. Thus, the initial agglomerate size distribution is also different.

This lack of stability can also be observed by the traditional method of direct visualization as shown in Figure 10. Pictures of the cuvette were taken with the nanofluid at the initial stage, after 4h and after the redispersion at 300ºC. When the particles are suspended in the fluid and well dispersed, the nanofluids look uniform and, in the case of the Al/Cu, completely dark. As the particles agglomerate and start to

settle, they move to the bottom of the cuvette and the fluid above becomes clearer. Finally, after the redispersion, the nanofluids should look homogeneous and similar to the initial stages as it can be noticed for both nanofluids, although only the Al/Cu nanofluid recovers its initial particle size distribution.

5. Conclusions

A new system suitable to measure the particle size distribution of nanoparticles suspended in a base fluid at high temperature conditions was set-up and calibrated. The system is composed of an external DLS device and a new cuvette specially designed to work up to 500ºC and compatible with molten salts.

The particle size distributions of silica nanoparticles dispersed in water and calcium nitrate tetrahydrate were measured from room temperature to 80ºC and compared to experimental results obtained in a low temperature DLS equipment commonly used in the literature. The good agreement between the results from both systems corroborate the suitability of the new high temperature DLS for the measurement of molten salt based nanofluids.

This device has allowed the measurement of the colloidal stability of molten salt based nanofluids for the first time. It was observed how silica nanoparticles agglomerate when dispersed in the different based fluids which have been tested: water, calcium nitrate and solar salt. The high ionic strength of the molten salts and the reduced Debye length lead to the formation of agglomerates due to the importance of the attraction forces over the electrostatic repulsion.

The evolution of the particle size distributions of molten solar salt containing silica and Al/Cu nanoencapsulated phase change material was measured for 4 h and after mechanical redispersion of the nanofluid at two different temperatures, 250ºC and

300ºC. For both nanofluids, there are initial agglomerates bigger than the colloidal stability limit previously calculated, which indicates the settling of the agglomerates. Stability curves and imaging over time corroborate the lack of stability of both nanofluids, although their initial particle size distributions were recovered after mechanical redispersion at 250ºC. Besides, the Al/Cu nanofluid presented smaller agglomerates than the silica nanofluid, it also shows lower agglomeration rate and the initial particle size distribution was recovered after redispersion of the sample at 300ºC.

Acknowledgements

This work has been partially funded by Ministerio de Economía y Competitividad (MINECO) through the project ENE2016-77694-R and by Universitat Jaume I through the project UJI-B2016-47. Nuria Navarrete thanks Universitat Jaume I for a pre-doctoral fellowship (FPI-UJI program) Ref. PREDOC/2016/28. JosepForner-Escrig thanks Ministerio de Economía, Industria y Competitividad and Fondo Social Europeo for a pre-doctoral fellowship Ref. BES-2017-080217. Authors thank Servicios Centrales de Instrumentacion Científica (SCIC) of Universitat Jaume I for the use of TEM (Maria del Carmen Peiro). This work has been developed by participants of the COST Action CA15119 Overcoming Barriers to Nanofluids Market Uptake (NANOUPTAKE).

References

1. Alva, G., Lin, Y., Fang, G.An overview of thermal energy storage systems. Energy 144 (2018) 341-378.

2. Mahian, O., Kianifar, A., Kalogirou, S.A., Pop, I., Wongwises, S.A review of the applications of nanofluids in solar energy. International Journal of Heat and Mass Transfer 57 (2013) 582–594.

3. Mondragon, R., Navarrete, N., Gimeno-Furio, A., Hernandez, L., Cabedo, L., Julia, J.E. Advances in New Heat Transfer Fluids From Numerical to Experimental Techniques. Chapter 11- New High-Temperature Heat Transfer and Thermal Storage Molten Salt–Based Nanofluids Preparation, Stabilization, and Characterization. Taylor & Francis Group, LLC. 2017

4. Serrano-López, R., Fradera, J., Cuesta-López, S. Molten salts data base for energy applications. Chemical Engineering and Processing 73 (2013) 87–102.

5. Bonk, A., Sau, S., Uranga, N., Hernaiz, M., Bauer, T. Advanced heat transfer fluids for direct molten salt line-focusing CSP plants. Progress in Energy and CombustionScience 67 (2018) 69-87.

6. Muñoz-Sánchez, B., Nieto-Maestre, J., Iparraguirre-Torres, I., García-Romero, A., Sala-Lizarraga, J.M. Molten salt-based nanofluids as efficient heat transfer and storage materials at high temperatures. An overview of the literature. Renewable and Sustainable Energy Reviews 82 (2018) 3924–3945.

7. Riazi, H., Murphy, T., Webber, G.B., Atkin, R., Mostafavi Tehrani, S.S., Taylor, R.A. Specific Heat Control of Nanofluids: a Critical Review. International Journal of Thermal Sciences107, 25-38 (2016).

8. Tiznobaik, H., Shin, D. Enhanced specific heat capacity of high-temperature molten salt-based nanofluids. International Journal of Heat and Mass Transfer57, 542-548 (2013).

9. Andreu-Cabedo, P., Mondragon, R., Hernandez, L., Martinez-Cuenca, R., Cabedo, L., Julia, J.E. Increment of specificheatcapacity of solar saltwith SiO2 nanoparticles. Nanoscale Res Lett. 9, 582–592 (2014).

10. Awad, A., Navarro, H., Ding, Y., Wen, D. Thermal-physical properties of nanoparticle-seeded nitrate molten salts. Renewable Energy 120 (2018) 275-288.

11. Mondragón, R., Juliá, J.E., Cabedo, L., Navarrete, N. On the relationship between the specific heat enhancement of salt-based nanofluids and the ionic exchange capacity of nanoparticles. Scientific Reports (2018) 8:7532.

12. Cingarapu, S., Singh, D., Timofeeva, E.V., Moravek, M.R. Nanofluids with encapsulated tin nanoparticles for advanced heat transfer and thermal energy storage. Int. J. Energy Res. 2014; 38:51–59.

13. Cingarapu, S., Singh, D., Timofeeva, E.V., Moravek, M.R., "Use of encapsulated zinc particles in a eutectic chloride salt to enhance thermal energy storage capacity for concentrated solar power", Renew. Ener., 80, 508-516 (2015).

14. Navarrete, N., Gimeno-Furio, A., Mondragon, R., Hernandez, L., Cabedo, L., Cordoncillo, E., Julia, J.E., "Nanofluid based on self-nanoencapsulated metal/metal alloys phase change materials with tuneable crystallisation temperature", Sci. Rep., 7, 17580 (2017).

15. H.E. Bergna, W.O. Roberts, Colloidal silica: Fundamentals and applications, CRC Taylor & Francis, 2006.

16. D.J. Shaw, Introduction to colloid and surface chemistry, Butterworth-Heinemann: Oxford, UK, 1991.

17. D. Quemada, C. Berli, Energy of interaction in colloids and its implication in rheological modelling, Adv. Colloid Interface Sci. 98 (2002) 51-85.

18. Mondragon, R., Julia, J.E., Barba, A., Jarque, J.C. Characterization of silica–water nanofluids dispersed with an ultrasound probe: A study of their physical properties and stability. Powder Technology 224 (2012) 138–146.

19. Zhang, H., Dasbiswas, k., Ludwig, N.B., Han, G., Lee, B., Vaikuntanathan, S., Talapin, D.V. Stable colloids in molten inorganic salts. NATURE, 542, 2017.

20. Gebbie, M.A., Smith, A.M., Dobbs, H.A., Lee, A.A., Warr, G.G., Banquy, X., Valtiner, M., Rutland, M.W., Israelachvili, J.N., Perkin, S., Atkin, R. Long range electrostatic forces in ionic liquids. Chem. Commun., 2017, 53, 1214.

21. Gebbie, M.A., Dobbs, H.A., Valtiner, M., Israelachvili, J.N. Long-range electrostatic screening in ionic liquids. Proceedings of the National Academy of Sciences of the United States of America (2015) 112(24), pp. 7432-7437.

22. Mondragón, R., Segarra, C., Martínez-Cuenca, R., Juliá, J.E., Jarque, J.C. Experimental characterization and modeling of thermophysical properties of nanofluids at high temperature conditions for heat transfer applications. Powder Technology 249 (2013) 516–529.

23. Gimeno-Furio, A., Navarrete, N., Mondragon, R., Hernandez, L., Martinez-Cuenca, R., Cabedo, L., Julia, J.E. Stabilization and characterization of a nanofluid based on a eutectic mixture of diphenyl and diphenyl oxide and carbon nanoparticles under high temperature conditions. International Journal of Heat and Mass Transfer 113 (2017) 908–913.

24. Torres-Mendieta, R., Mondragon, R., Puerto-Belda, V., Mendoza-Yero, O., Lancis, J., Julia, J.E., Mínguez-Vega, G. Characterization of Tin/Ethylene Glycol Solar Nanofluids Synthesized by Femtosecond Laser Radiation. ChemPhysChem 2017, 18, 1055 – 1060.

25. Torres-Mendieta, R., Mondragon, Julia, J.E., Mendoza-Yero, O., Cordoncillo, E., Lancis, J., Mínguez-Vega, G. Fabrication of gold nanoparticles in Therminol VP-1 by laser ablation and fragmentation with fs pulses. Laser Phys. Lett. 11 (2014) 126001 (6pp).

26. Jo, B., Banerjee, D. Enhanced specific heat capacity of molten salt-based nanomaterials: Effects of nanoparticle dispersion and solvent material. Acta Materialia (2014) 75: 80–91.

27. Kuchibhatla, A., Karakoti, A.S., Seal, S. Colloidal Stability by Surface Modification. JOM (2005) 52-56.

28. Park, S-J., Seo, M-K. Intermolecular Force. Chapter 1 in Interface Science and Composites. Interface Science and Technology 18 (2011) 1-57.

29. Bergstrom, L. Colloidal Processing of Ceramics. Chapter 9 in Handbook of Applied Surface and Colloid Chemistry. 2001 John Wiley & Sons, Ltd.

30. Griffin, G.P., Jurinak, J.J. Estimation of activity coefficients from the electrical conductivity of natural aquatic systems and soil extracts. Soil Science 116 (1973) 26–30.

31. Ohshima, H. Interaction of colloidal particles. Colloid and Interface Science in Pharmaceutical Research and Development (2014), 1-28.

32. Liang, Y., Hilal, N., Langston, P., Starov, V. Interaction forces between colloidal particles in liquid: Theory and experiment. Advances in Colloid and Interface Science 134–135 (2007) 151–166.

Figure captions

Figure 1. *Experimental set-up for external high temperature DLS measurements.*

Figure 2. *Particle size distributions of water and $Ca(NO_3)_2$ based silica nanofluids.*

Figure 3. *Colloidal stability limit of the nanofluids. Brownian motion and Stokes sedimentation influence on a) Water-SiO_2 nanofluids b) $Ca(NO_3)_2$-SiO_2 nanofluid c) Solar salt-SiO_2 nanofluid and d) Solar salt-Al/Cu nanofluid.*

Figure 4. *TEM micrographs of a) SiO_2 and b) Al/Cu nanoparticles.*

Figure 5. *Particle size distributions of primary silica nanoparticles (TEM) and dispersed in different base fluids (DLS).*

Figure 6. *Diagram of electric double layer.*

Figure 7. *Evolution of particle size distributions through time and with redispersion for a) and c) SS-SiO_2 and b) and d) SS-Al/Cu at 250ºC.*

Figure 8. *Evolution of particle size distributions through time and with redispersion for a) and c) SS-SiO_2 and b) and d) SS-Al/Cu at 300ºC.*

Figure 9. *Evolution of zeta potential with pH for SiO_2 and Al/Cu dispersed in 1% solar salt aqueous solution.*

Figure 10. *Evolution of nanofluid visual sedimentation through time and with redispersion at 300ºC.*

Table captions

Table 1.*Comparison of $D_{i,50}$ of different nanofluids and DLS devices.*

Table 2.*Electrical conductivity, ionic strength, Debye length, and cluster size.*

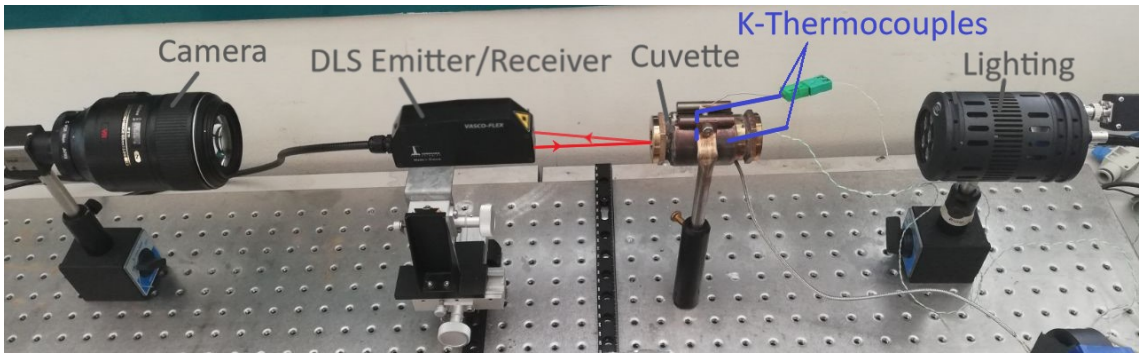

Figure 1.*Experimental set-up for external high temperature DLS measurements.*

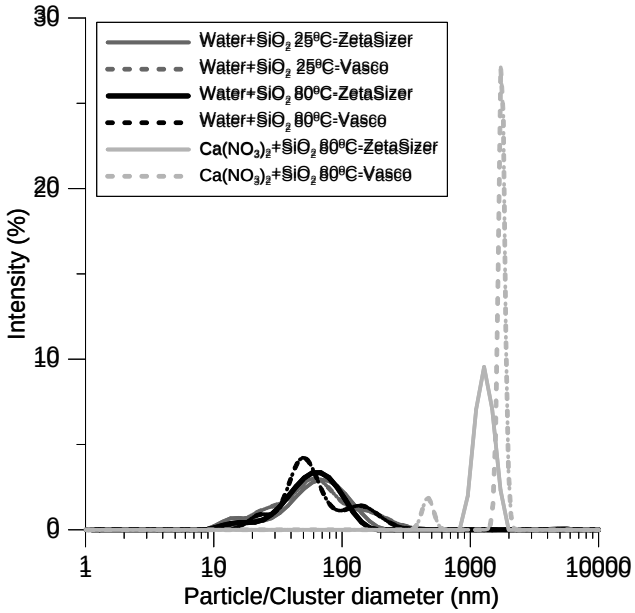

Figure 2.*Particle size distributions of water and $Ca(NO_3)_2$ based silica nanofluids.*

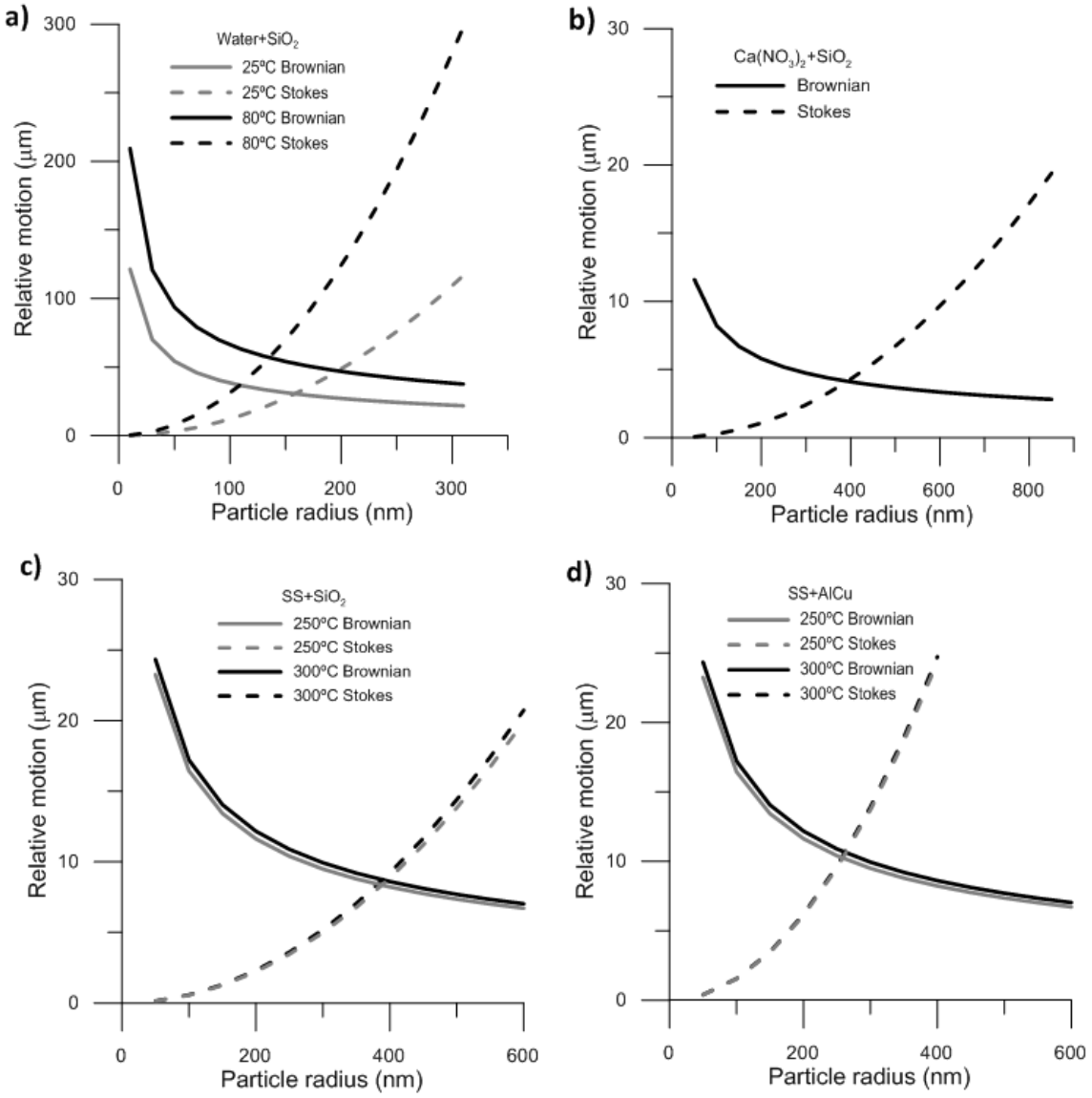

Figure 3. *Colloidal stability limit of the nanofluids. Brownian motion and Stokes sedimentation influence on a) Water-SiO_2 nanofluids b) $Ca(NO_3)_2$-SiO_2 nanofluid c) Solar salt-SiO_2 nanofluid and d) Solar salt-Al/Cu nanofluid.*

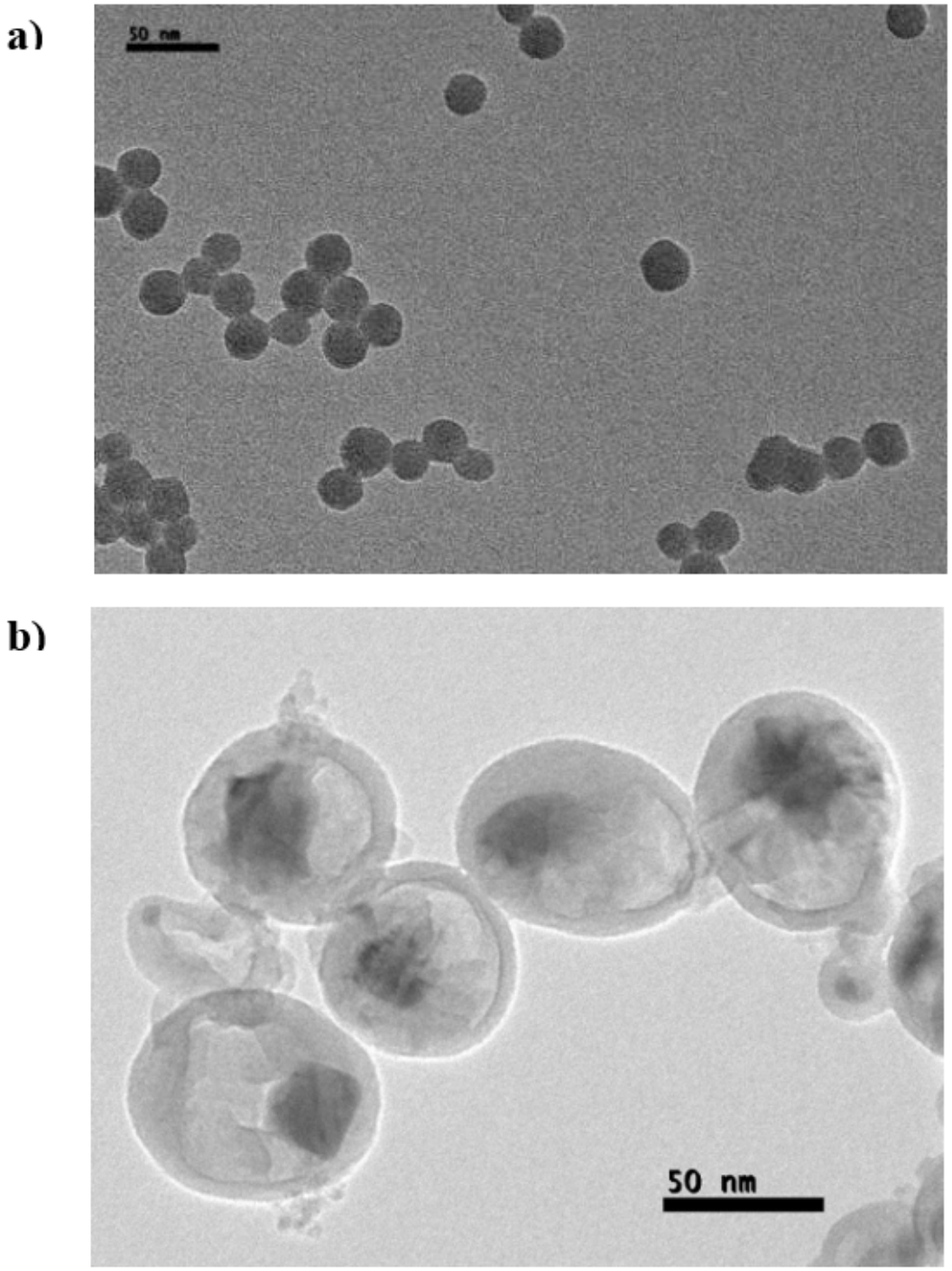

Figure 4. *TEM micrographs of a) SiO_2 and b) Al/Cu nanoparticles.*

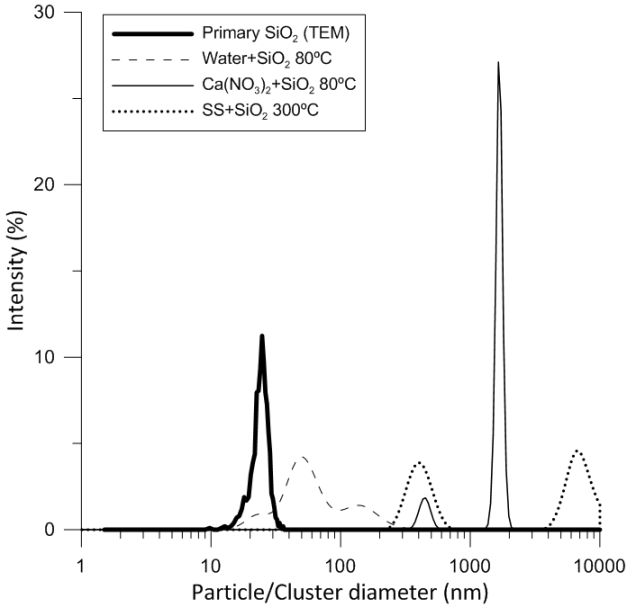

Figure 5. *Particle size distributions of primary silica nanoparticles (TEM) and dispersed in different base fluids (DLS).*

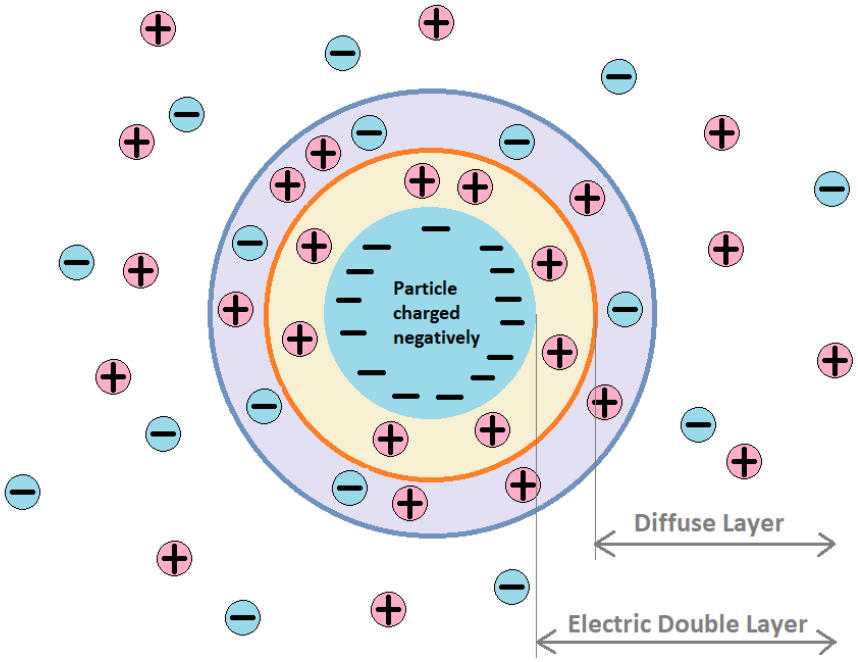

Figure 6. *Diagram of electric double layer.*

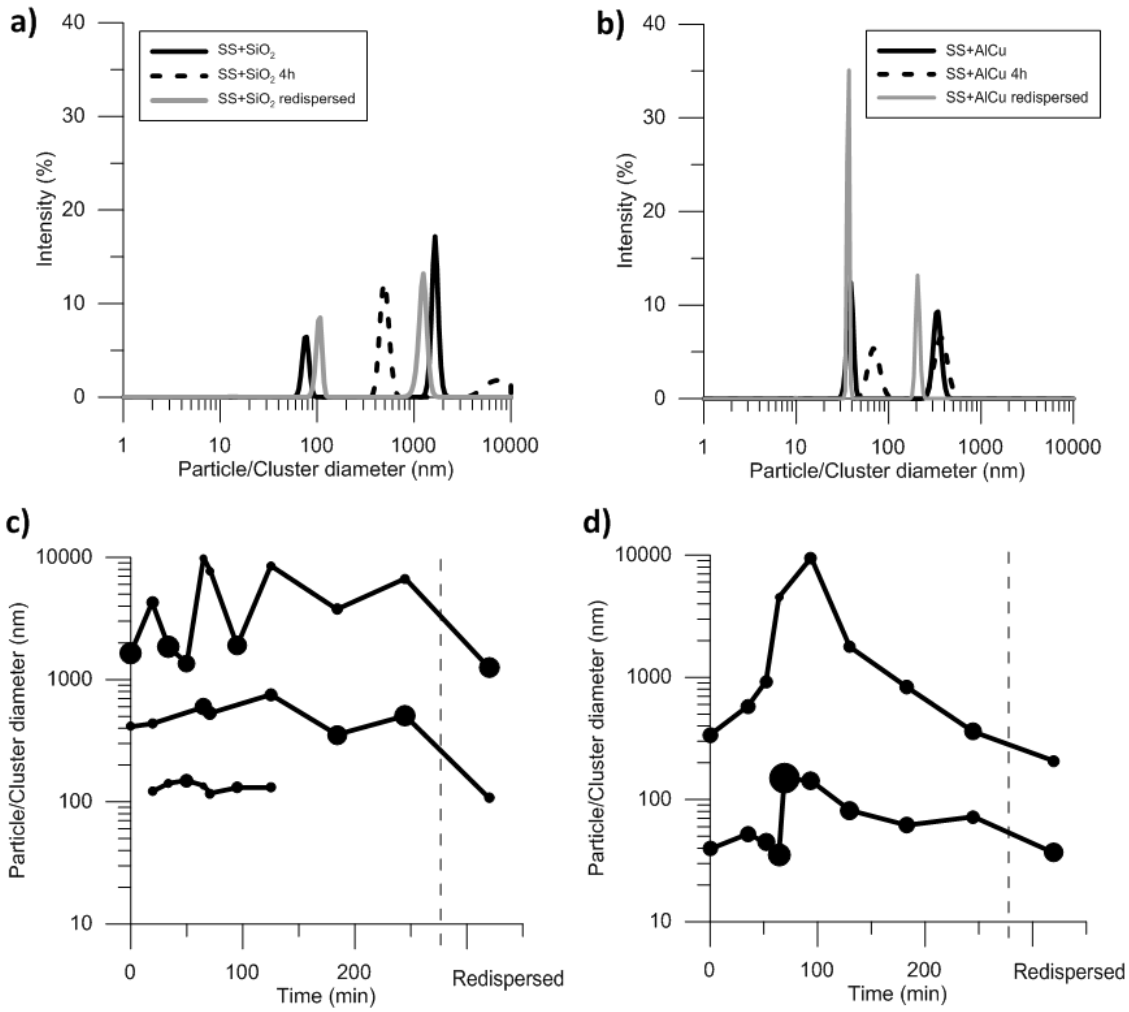

Figure 6. *Evolution of particle size distributions through time and with redispersion for a) and c) SS-SiO_2 and b) and d) SS-Al/Cu at 250ºC.*

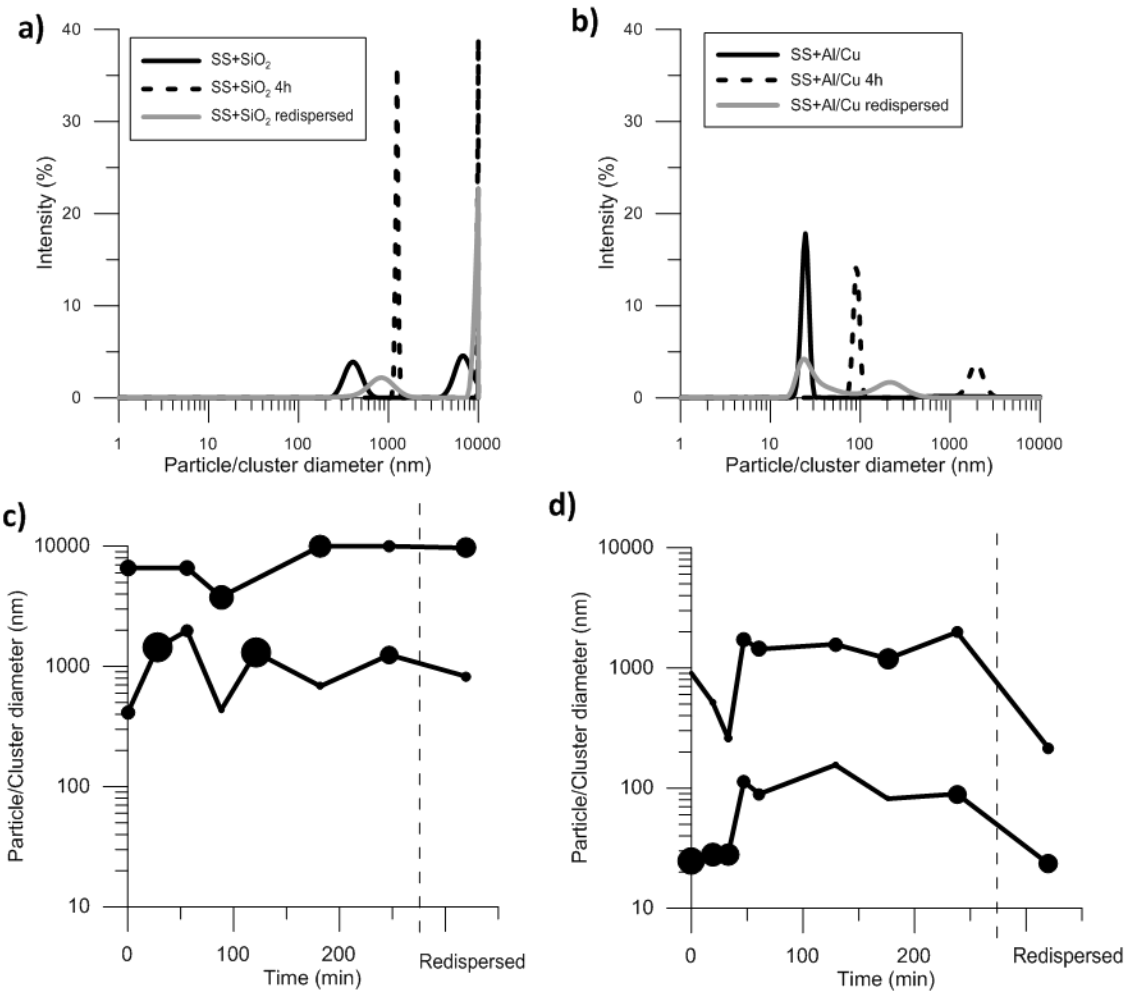

Figure 7. *Evolution of particle size distributions through time and with redispersion for a) and c) SS-SiO_2 and b) and d) SS-Al/Cu at 300ºC.*

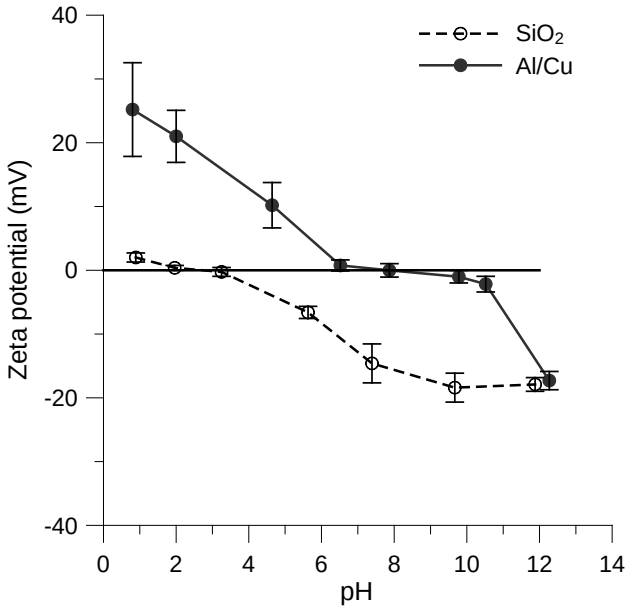

Figure 9. *Evolution of zeta potential with pH for SiO_2 and Al/Cu dispersed in 1% solar salt aqueous solution.*

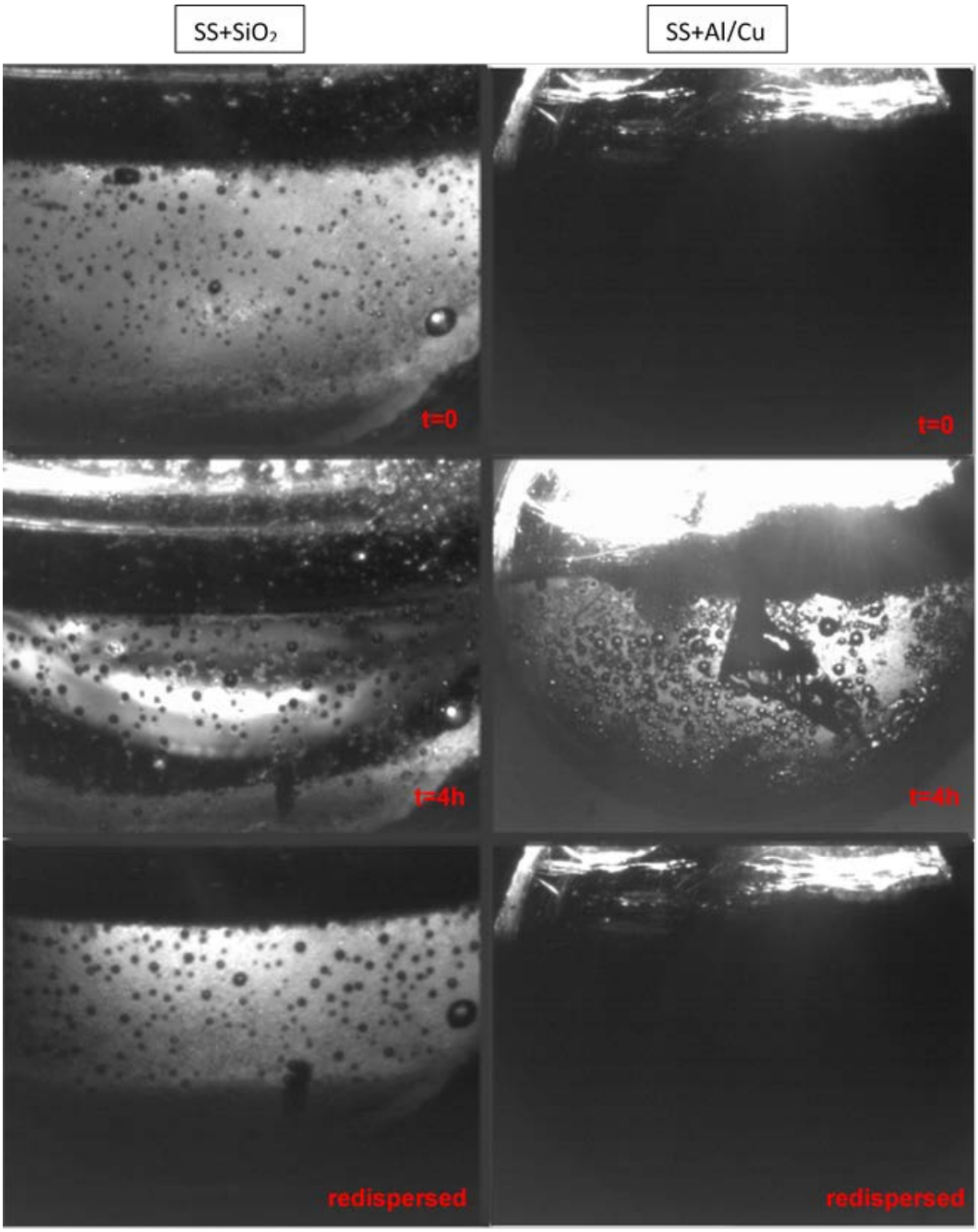

Figure 10. *Evolution of nanofluid visual sedimentation through time and with redispersion at 300ºC.*

Table 1. *Comparison of $D_{i,50}$ of different nanofluids and DLS devices.*

Sample	$D_{i,50}$ (nm) VASCO FLEX	$D_{i,50}$ (nm) ZetaSizer	Error (%)
Water+SiO_2 25ºC	61.83	60.40	2.37
Water+SiO_2 80ºC	56.36	60.80	7.30
$Ca(NO_3)_2$+SiO_2 80ºC	1647.66	1590.00	3.63

Table 2.*Electrical conductivity, ionic strength, Debye length, and cluster size.*

	EC (mS/cm)	**I (mol/L)**	**κ^{-1} (nm)**	**D_i (nm)/Intensity (%)**	
				Peak #1	Peak #2
Water+SiO_2 25ºC	0.605	0.008	3.425	61.83/3.2	-
Water+SiO_2 80ºC	1.140	0.015	2.397	51.39/4.2	142.11/1.4
$Ca(NO_3)_2$+SiO_2 80ºC	6.540	31.128	0.017	451.46/1.9	1647.66/27.1
SS+SiO_2 300ºC	-	20.910	0.023	392.99/3.9	6595.95/4.5